12 Physics of Biological Systems

Cornel Andreoli, Conrad Escher, Hans-Werner Fink, Michael Krüger,
Tatiana Latychevskaia, Hiroshi Okamoto, Gregory Stevens.

in collaboration with:
Jevgeni Ermantraut, Clondiag Chip Technologies (Germany); Pierre Sudraud, Orsay Physics (France); Roger Morin, CNRS Marseille (France); John Miao, University of California at Los Angeles (USA); Dieter Pohl, University of Basel; Andreas Plückthun, Peter Lindner, Biochemistry Institute, University of Zurich; Bettina Böttcher, EMBL-European Institute for Molecular Biology, Heidelberg; Andre Geim, Centre for Mesoscience & Nanotechnology, University of Manchester.

In connection with the structural investigation of biological objects by Low Energy Electron Point Source (LEEPS) microscopy we established a reliable sample preparation technique to be able to investigate single phage molecules. Holograms of single molecules have been recorded and numerically reconstructed. The reconstructed images have been compared with TEM images of the same molecule which was very useful to validate the numerical reconstruction step. A European NEST ADVENTURE grant proposal has been accepted for funding, our group being the leading partner within a European consortium. After significant technical improvements of our low-temperature LEEPS microscope, electron holograms could be recorded from carbon fibers at liquid He temperature. The numerical routine for hologram reconstructions has been improved and allows now the simultaneous retrieval of absorption and phase shifting properties of the holographically recorded object with the consequence that transparent phase objects can be reconstructed from holograms. After the successful development of a new ion source based on the solid electrolyte (AgI)($AgPO_3$), which has been reported last year, studies on the conduction mechanism have been performed. Direct experimental evidence for the existence of ion conduction pathways has been found by observing the emission patterns of a sharp solid electrolyte tip in a field ion microscope. A new field emission microscope has been built in the framework of the advanced practical student courses in physics to observe and analyse the motion of Cs atoms on a W (110) surface.

12.1 Structure of individual biological molecules

Gregory Stevens, Michael Krüger and Hans-Werner Fink
in collaboration with: Andreas Plückthun and Peter Lindner of the Biochemistry Institute

The objective of this project is to acquire in-line electron holograms of individual molecules, from which an image of the molecule can be numerically reconstructed. In order to present the molecule to the coherent electron wave, it must be prepared so that electrons are scattered by the molecule, with minimum disturbance from a supporting substrate. One way of doing this is to use a filamentous molecule that has been suspended across a hole in a supporting film. The molecule chosen for these experiments is a mutant of filamentous bacteriophage called f1K. This was chosen because not only can it be placed in the electron beam, but it may also be used as a convenient scaffold to present other molecules to the electrons.

Since April 2005, we have obtained electron holograms of a single f1K using a purpose-built Low Energy Electron Point Source (LEEPS) microscope. This microscope is called the bioLEEPS, and was designed and constructed for imaging biological molecules. From these holograms, numerically reconstructed images of the phage were obtained and compared to a transmission electron microscope (TEM) image of the same phage. Although the resolution of the image does not provide detailed structural information about the phage, it is nevertheless encouraging that the size and shape of the object image obtained by holography is in good agreement with the size and shape of the image obtained with the TEM.

A new development in the preparation of the phage is that the specimen is more quickly frozen than before. This seems to prevent the phage forming bundles of two or more phage particles across the hole in the support film. An understanding of the need to rapidly freeze the specimen, to encourage the formation of amorphous rather than crystalline ice, came about during a visit to the lab of Prof. Kühlbrandt at the Max Planck Institute for Biophysics in Frankfurt (Main).

A TEM micrograph of an individual free-standing phage is shown in Fig. 12.1 (a). The width of the filament, 7.5 nm, indicates that

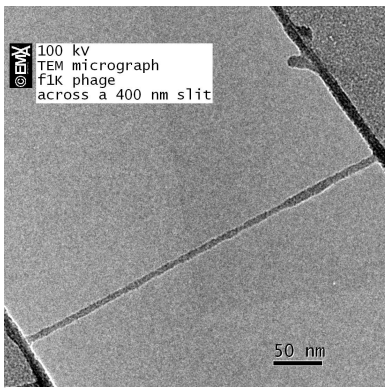

(a): 100 kV TEM micrograph of a single f1K phage suspended across a 400 nm wide slit in a carbon film.

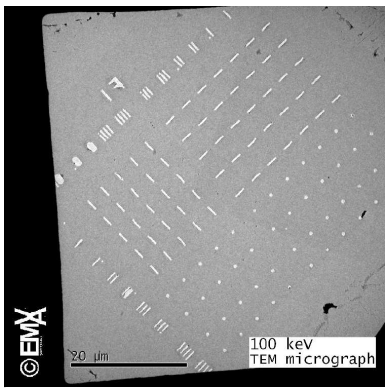

(b): a micro machined carbon support film with an array of addressable slits.

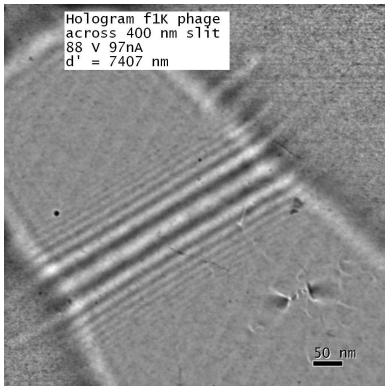

(c): a hologram of the same phage in (a), recorded with an electron energy of 88 eV.

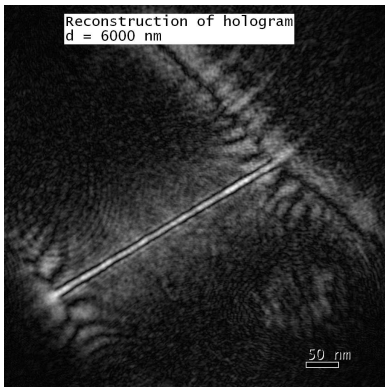

(d): numerically reconstructed image from the hologram in (c) obtained with software developed by Dr.Tatiana Latychevskaia.

Figure 12.1: We gratefully acknowledge the Institute of Veterinary Anatomy and Virology, University of Zurich for the use of their facilities in making the TEM images.

this is an image of a single phage, rather than a bundle of two or more strands. Another new development is the use of a carbon support film with holes and slits that are addressable, as shown in Fig. 12.1 (b). These special support membranes are prepared in our lab with a state-of-the-art focussed ion beam system. With this kind of support film, it is relatively easy to locate the same molecule so that it can be imaged in both the TEM and the LEEPS microscope.

The phage shown in Fig. 12.1 (a) was placed in the LEEPS microscope at a distance of 7.4 μm from a point source of coherent electrons so that a high contrast in-line electron hologram was cast on a detector screen located 100 mm away. The resulting hologram is shown in Fig. 12.1(c). The phage structure, depicted in Fig. 12.1 (d) as the amplitude of the reconstructed object wave, was obtained numerically, and shows the phage magnified by a factor of about 1.1×10^5.

Images of the phage obtained using the TEM and by numerically reconstructing the hologram are shown in Fig.12.1 (a) and (d). It was possible to compare the two imaging methods because the same molecule was located using the addressing system for the slit. In these images, it can be seen that the ratios of the width to the length of the filament are in good agreement, as are variations in the width of the molecule along its length.

We studied the effect of varying the distance between the electron source and the specimen on the formation of holograms. It is clear from these experiments, together with simulations of electron trajectories near an uncharged filament, that there is a lower limit in the source-specimen distance, beyond which the holograms cannot be reconstructed with the presently available software. This lower limit appears to depend on the experimental conditions, including the diameter of the filament being imaged.

It has been possible to obtain and reconstruct electron holograms of an individual phage. It is now a matter of extending these studies towards structural biology of single molecules. We envision proceeding towards this goal by employing the phage as a scaffold to bind single molecules to its protein shell.

As a first step towards this goal, we have succeeded in binding mono N-Hydroxy Succinimide (NHS) gold nanoparticles to the protein coat of the phage without causing the phage to cross-link and form aggregates. We found that it is necessary to keep the ratio of nanogold particles to phage binding sites to a value of less than one so as not to overload the phage with gold nanoparticles. The next step will be to obtain holograms of the nanogold particles attached to the phage. Once it has been established that the nanogold particles can be imaged on the phage coat by electron holography, we plan to extent this technique to attach biological proteins of interest to the phage. Initial experiments in this direction will focus on binding green fluorescent protein to the phage with NHS cross linker molecules.

Apart from the challenge associated with presenting single molecules to the coherent electron wave, various improvements in the instrumentation and hologram reconstruction routine are needed towards obtaining three-dimensional high resolution data on single biological molecules. We plan to begin this by improving the sensitivity of the data collection system: a fibre optic plate will be employed to couple the detector screen directly to the chip of the CCD camera.

12.2 The SIBMAR project

Hans-Werner Fink, Tatiana Latychevskaia, Gregory Stevens and Michael Krüger
in collaboration with: Andreas Plückthun of the Biochemistry institute, Andre Geim of Manchester University and Bettina Böttcher of EMBL Heidelberg

We formed a consortium with two other European partners: groups headed by Prof. Andre Geim of the University of Manchester and Dr. Bettina Böttcher of the EMBL in Heidelberg, and applied for a European NEST ADVENTURE grant to develop LEEPS microscopy for imaging biological macromolecules at atomic resolution. This proposal was called SIBMAR, and in January 2006 it was awarded funding for up to five postdoctoral positions for three years.

The main objective of this project, to obtain structural information about individual biological macromolecules at atomic resolution, will be accomplished by tackling the following sub objectives:

- An atomically thin carbon support substrate will be developed by Prof. Geim's group.
- The effects of low energy electrons on biological molecules will be studied by Dr. Böttcher's group.
- Prof. Plückthun's group will develop methodologies for preparing individual bio molecules.
- Dr. Latychevskaia, of Prof. Fink's group, will develop numerical reconstruction routines for recovering three-dimensional images from a set of holograms.
- Others in Prof. Fink's group will develop a prototype LEEPS microscope for obtaining high resolution holograms.

We are now in the process of negotiating a contract with the European Commission and expect that the project will begin around the middle of 2006.

12.3 The cryogenic LEEPS project

Hiroshi Okamoto and Hans-Werner Fink

The construction of the cryogenic low energy electron point source microscope (cryo-LEEPS) has come to a successful conclusion during the last year. Although the microscope has been capable of imaging for more than a couple of years, numerous improvements on electro-static environment, magnetic shield, and cooling system among others resulted in high enough reliability of the instrument as well as sufficient image quality at low temperatures that finally allowed for publication of the technical description of the microscope (1). The microscope (Fig.12.2) is one of the only two currently existing helium-temperature LEEPS systems in the world. The other one developed by Dr. B. Cho of Prof. Oshima's group at Waseda University in Japan (2) allows for cooling of the field emitter.

One unique feature of our system is that the whole microscope including the imaging screen is immersed to liquid helium to guarantee sufficient cooling of the specimen. The reason is as follows. Viewed from the specimen-emitter assembly, the imaging screen spans a considerable solid angle. According to Stefan-Bolzmann's law, infrared radiation heat flux is proportional to T^4, and clearly we must cool the screen down to cryogenic temperature to

stop large radiation heat influx to the specimen. Indeed, we have observed a significantly higher degree of charge-up of a lacey carbon specimen at liquid helium temperature (Fig. 12.3 c) but not at room temperature (Fig. 12.3 a) or at liquid nitrogen temperature (Fig. 12.3 b): Such a significant change with temperature had not been reported before. Moreover, it was found that charging was not observed near the metallic grid supporting lacey carbon film at liquid helium temperature. This fact underscores the notion that

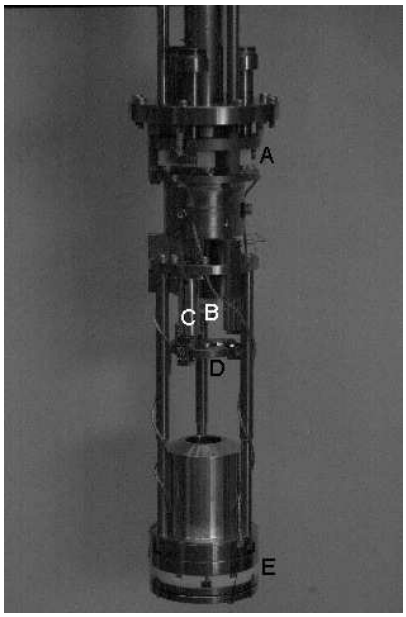

Figure 12.2: The LEEPS microscope unit. (A) The cryogenic connector. (B) The field emitter. (C) The tube piezo as a part of the Besocke stepper, hidden inside the aluminium shield. (D) The Besocke plate, on which specimens are mounted. (E) The screen assembly consisting of a metallic mesh and a phosphor screen. The copper tube above the screen assembly prevents stray electrons from reaching the screen.

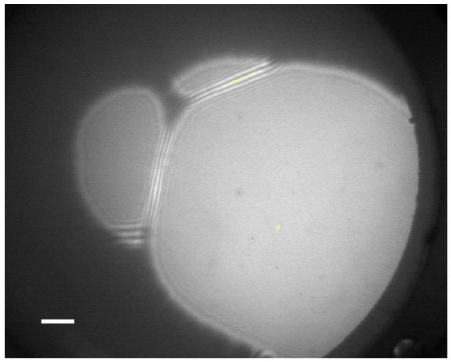

(a)

Carbon fibers at room temperature.

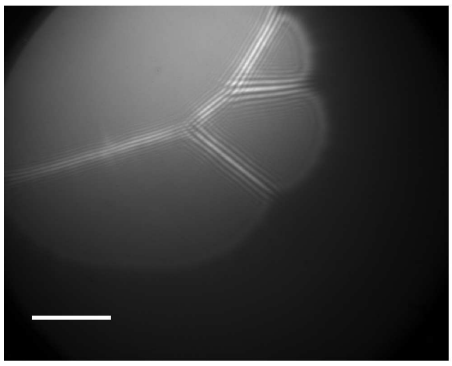

(b)

An image taken at liquid nitrogen temperature.

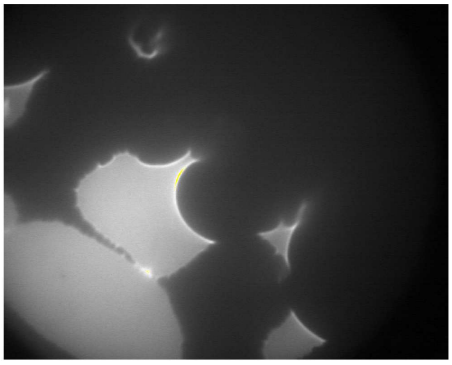

(c)

At liquid helium temperature, carbon film appears to become rather insulating.

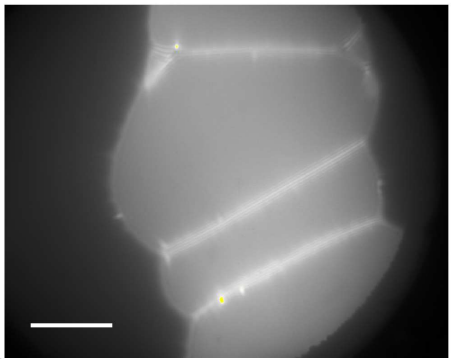

(d)

At places close to the supporting gold 400 mesh grid, interference fringes are still visible.

Figure 12.3:
LEEPS images of a lacey carbon film. The horizontal bars in (a), (b), and (d) indicate estimated 100 nm, 100 nm, and 500 nm scales, respectively, as deduced from the Fresnel fringes seen in these images. The electron energies were 80 eV, 65 eV, 85 eV, and 65 eV for (a)-(d), respectively.

electron conductivity of the specimen and/or substrate is of importance at low temperatures. Additionally, we have introduced a method to estimate scale of images based only on the observed Fresnel fringe spacing and known electron energy. This method is particularly useful for a LEEPS system under variable temperature conditions. Based on the method, the scale of the horizontal bars in Fig. 12.3 were estimated to be 100 nm, 100 nm, and 500 nm, respectively.

In line with the group's interest in visualizing electrical conduction in nanoscale objects, this instrument should be ideal to study, for example, the transition of electrical conduction mechanism from thermal excitation to quantum mechanical hopping.

[1] H. Okamoto and H.-W. Fink, Rev. Sci. Instrum. 77, 043714 (2006).
[2] B. Cho *et al.*, Rev. Sci. Instrum. 75, 3091 (2004).

12.4 Numerical hologram reconstruction

Tatiana Latychevskaia and Hans-Werner Fink

An in-line hologram is recorded as following. A single molecule is placed in a divergent beam of coherent electrons, and a magnified shadow of the molecule appears on a detector screen. The image is a hologram, which is formed by the interference of two electron waves: those which are scattered by the molecule (object wave) and those which are not scattered (reference wave). The hologram can be used to numerically reconstruct the field distribution at different distances from the screen, giving the molecule's shape at various distances. By combining this information, the 3-dimensional shape of the molecule can be rendered. The final goal is to retrieve the three-dimensional shape of a biological molecule at a few $\mathring{A}$ resolution.

In the previous year, the numerical routine for hologram reconstructions was developed. In the last year this routine was improved so that phase objects, which are transparent for the electron beam, could be reconstructed from holograms. The present reconstruction routine allows simultaneous retrieval of absorption and phase properties of the holographically recorded object.

To validate our phase reconstruction method experimentally, we recorded optical holograms of a microscopic glass sample with engraved psi-letters in it. For both, pure amplitude and pure phase objects, a 10 nm thin layer of ITO was deposited onto a round glass cover slide (thickness of about 0.15 mm) by e-beam evaporation. For the pure amplitude object, additional layers of titanium (1.5 nm) and then gold (20.5 nm) were deposited onto the ITO layer. The psi-letter was then formed by removing parts of titanium and gold with a focussed ion beam machine (FIB). For the pure phase object, a psi-letter was engraved in the ITO layer and the under laying glass.

Fig. 12.4 a) shows a hologram of an area of the glass piece where both objects, amplitude and phase psis are engraved. Fig. 12.4 b) shows the reconstructed absorption distribution and Fig. 12.4 c) shows the reconstructed phase distribution. While the *amplitude psi-letter* appears sharp on the reconstructed absorption distribution, it appears out of focus on the reconstructed phase distribution, and the *phase psi-letter* is only visible in the reconstructed phase distribution.

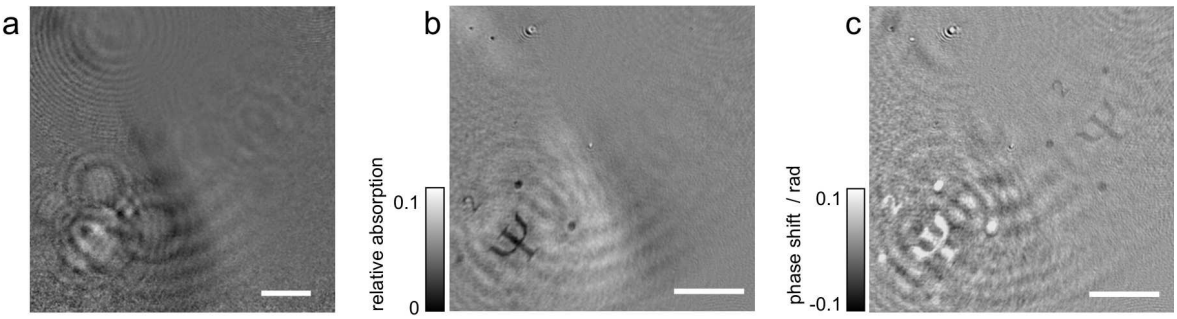

Figure 12.4:
a) Hologram of a glass area with two psis engraved , one is a pure amplitude and the other one is a pure phase object; the size of the area is about 300×300 mm^2. The scale bar is about 50 mm.
b) Reconstructed absorption distribution.
c) Reconstructed phase distribution. The size of the reconstructed area is about 435×435μm^2.
The scale bars in b) and c) are about 100 μm.

The developed numerical routine is especially important for reconstruction of holograms of biological objects, as biological objects demonstrate both, absorption and phase shifting properties when recorded with low energy electrons (100-200 eV).

12.5 Studies on the Conduction Mechanism in a Solid Electrolyte

Conrad Escher, Cornel Andreoli, Tatiana Latychevskaia and Hans-Werner Fink

in collaboration with: Dieter Pohl, Physics Institute, University of Basel

Having developed a solid electrolyte ion source for focused ion beam applications, the source is eventually used as a tool to study the conduction mechanism in solid electrolytes.

In a good solid-electrolyte, the mobile ions can move almost as freely as in a liquid. The resulting DC and AC conduction in solid state devices of the type shown in Fig. 12.5 (a) has been studied extensively (1; 2). However, details about the microscopic conduction mechanism in solid electrolyte conductors are experimentally not directly accessible. If, on the other hand, the solid electrolyte is given the shape of a sharp tip, set on high potential with respect to some counter electrode, ions of the mobile species may be field emitted and detected on a screen of a field ion microscope (3). This opens up the possibility to measure the emission current (4) and to observe the emission dynamics. In this way, direct insight into the conduction mechanism can be obtained. Here we report on such an experiment with a source made of amorphous $(AgI)_{0.5}(AgPO_3)_{0.5}$.

The fabrication of this solid electrolyte is fairly easy and it can readily be shaped into a sharp tip. Furthermore, its conductivity at room temperature is one of the largest known ($\sigma \approx 10^{-2}$ S/cm at 25^{o}C) (5; 6) . Contacting the tip to a silver wire or fixing it with silver paste to the source holder provides a silver reservoir, which is required for continuous operation. The solid electrolyte tip is incorporated into a field ion microscope (Fig. 12.5 (b)). When a high voltage is applied between tip and detector, Ag^+ ions are field emitted from the solid electrolyte and accelerated onto the detector. The ion emission signal is finally transferred into a light signal on a fluorescent screen as shown in Fig. 12.5 (c). A highly magnified image

of the emission sites at the tip apex is observed and the dynamics of the emission patterns on the screen are recorded by a video camera. With this technique, we address the question of the conduction mechanism in amorphous electrolytes.

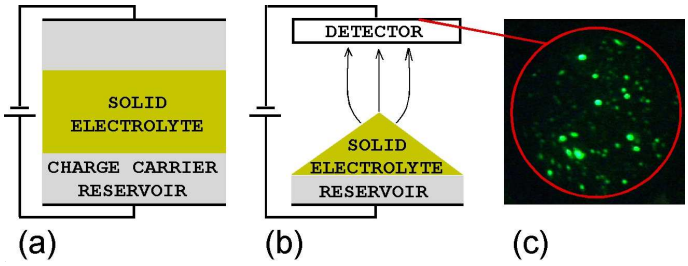

Figure 12.5: Schematic setups to measure ion conduction properties. (a) Electrolytic cell, allows time-resolved measurements, but on a macroscopic scale. (b) Field ion microscope with a solid electrolyte as source allows time- and spatially resolved measurements of a microscopic area. (c) The ion emission signal from an $(AgI)_{0.5}(AgPO_3)_{0.5}$ tip, recorded with a video camera at a frequency of 25 Hz.

Theory predicts that the mobile ions move in conduction *pathways* (6)-(15) but experimental evidence has been indirect only. In amorphous $(AgI)_x(AgPO_3)_{1-x}$ (5,6) with x≈ 0.5, chosen for our investigation, it is believed that the pathways are made up of the highly conductive AgI respectively its Ag^+ ions which squeeze between the glass-forming, less conductive $AgPO_3$ chains. This expands the glass network which might explain the existence of a *first sharp diffraction peak* in the neutron diffraction spectrum at unusually small momentum transfer (12)- (16). Above concentrations x≈0.3, cluster-like regions percolate into extended channels (5)- (7). This allows hopping of Ag^+ through the whole solid-electrolyte. Extended numerical simulations of the atomic arrangement in the ionic glass structure confirm this picture (9; 10). They lead to a refined model where the conduction pathways are created by the dynamic response of the $AgPO_3$ network to the occupation of mobile cation sites by Ag^+. The relaxation of the network is slow compared to the hopping attempt frequency; the network structure thus persists for some time after an ion has hopped to the next site. This leaves a trace for more ions to follow its path.

We shall first describe experimental observations consistent with the model outlined above. Thereafter, we present quantitative data that provide direct experimental evidence for the existence of ion conduction pathways. As apparent from Fig. 12.5 (c), the emission does not originate from a single, large spot as one might have expected for a tip surface that appears completely smooth in the electron microscope (4). Instead it consists of a number of bright spots as small as 3 nm in diameter. As evident from the sequence in Fig. 12.6, cooling the tip with liquid nitrogen decreases the number of spots and the emission current to almost zero. This demonstrates that a thermally activated process is responsible for the rate of ion emission - in agreement with theory predicting a temperature-dependent mobility of ions being the important rate-limiting factor (8). Upon cooling, the number of emission sites decreases while the intensities of the remaining sites stabilize. In view of the conduction pathway model, it ap-

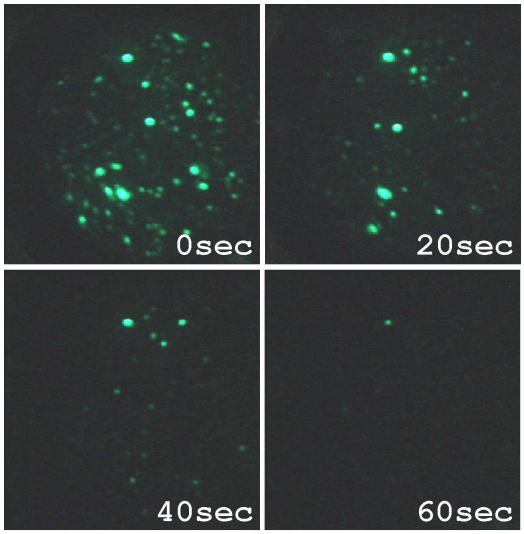

Figure 12.6: Qualitative observation of the temperature dependence of the ion conductivity. The sequence shows the decay of the emission spot intensities at constant voltage upon cooling down by liquid nitrogen to an estimated final temperature of about 100 K.

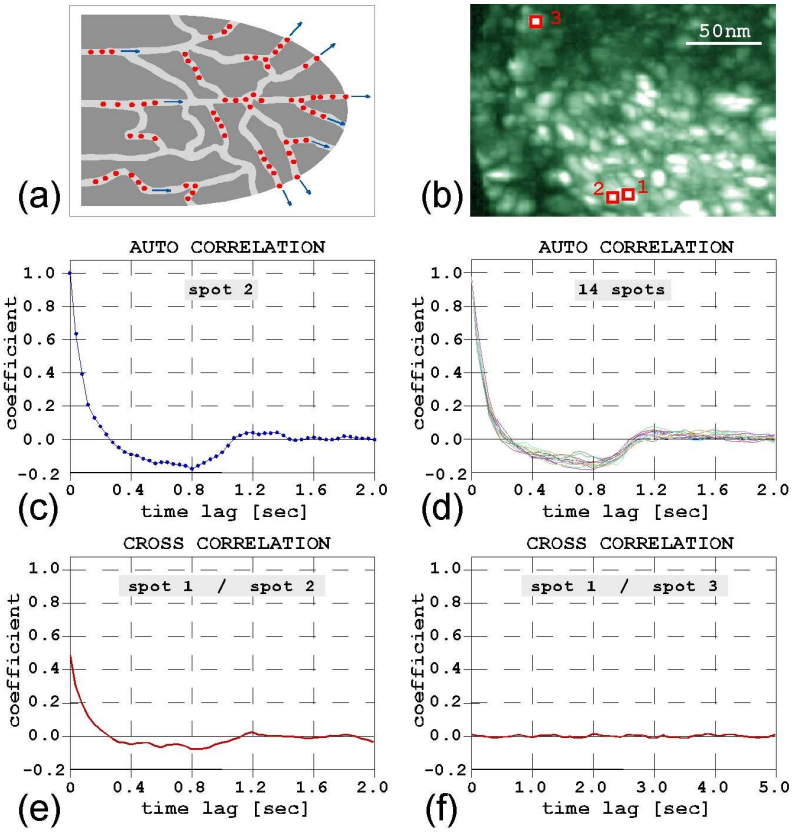

Figure 12.7: Quantitative evaluation of the silver ion emission patterns. (a) Schematic cut through an ion emitter tip exhibiting a network of ion channels. (b) The superposition of 3000 video frames clearly shows the existence of distinct emission spots at the tip apex. Three out of a total of 14 spots for further analysis of their intensities as a function of time have been marked by red squares. (c) The intensity auto-correlation function for spot 2 with a temporal resolution of 40 ms. (d) The auto-correlation functions for 14 individual spots. (e) Cross-correlation between two neighboring spots (1 and 2) 10 nm apart. (f) Cross-correlation between two spots (1 and 3) separated by a distance of 130 nm.

pears plausible that not only the mean hopping attempt frequency is reduced when the electrolyte is cooled down but also the relaxation time of the surrounding network structure is prolonged. As a consequence, only the most pronounced pathways remain active and lead to stabilized currents for the reduced overall flux of Ag^+ ions.

It is interesting to note that the emission current of a $(AgI)_{0.5}(AgPO_3)_{0.5}$ tip needs a few minutes to build up, and hysteresis in the I/V-characteristics was observed (4). This, again in view of the pathway model, indicates that the development of conduction pathways to the apex is not instantaneous.

However, the most direct indication for ion emission from individual end points of conduction pathways, as sketched in Fig. 12.7 (a), is the fact that the emission patterns consist of a number of distinct spots with smallest diameters and separations of the order of 3 nm. Even after a superposition of 3000 consecutive emission patterns, equivalent to an integration over 2 minutes, the discrete nature of the emission is preserved (Fig. 12.7 (b)). Given this distinct spatial distribution of emission sites, the observed fluctuations in the overall ion signal must be due to fluctuations within individual sites.

The analysis of the time dependence of these microscopic currents shall provide insight into the dynamics of charge transport within individual pathways. To explore this, we measured the intensity auto-correlation function for 14 individual spots. The current versus time signal has been evaluated by monitoring the relative detector intensities of individual spots. For each spot the auto-correlation function f has been computed according to:

$$f(\Delta t) = \frac{1}{N-\Delta t} \sum_{t=0}^{N-\Delta t} \frac{(I(t)-\overline{I})(I(t+\Delta t)-\overline{I})}{(I(t)-\overline{I})^2} \qquad (12.13)$$

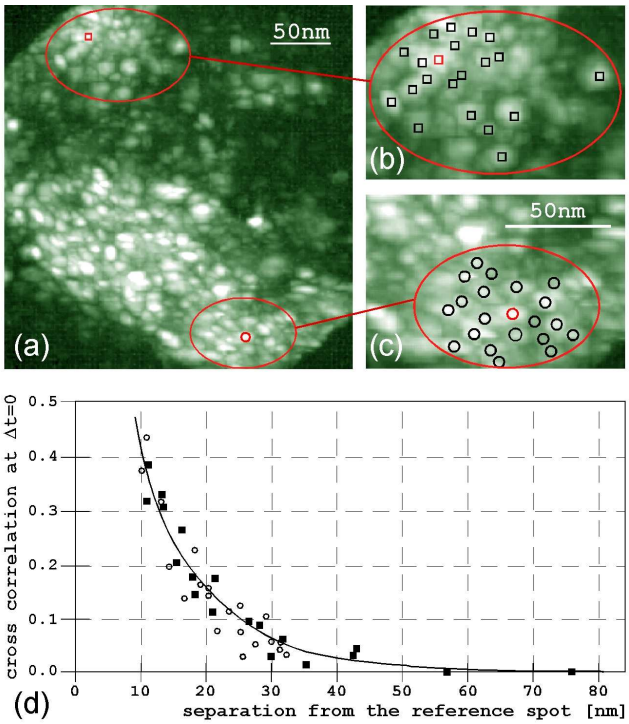

Figure 12.8: Distance dependence of the cross correlation. (a) Emission pattern from which two different regions have been arbitrarily chosen for further analysis. (b,c) In these two regions, the cross correlation function at δt=0 has been evaluated for several spots at different distances in respect to a reference spot, marked in red. (d) The two data sets (circles and squares) represent the decay of the cross-correlation for the two regions on the apex of the solid electrolyte ion source.

where I(t) is the intensity at time t, $\overline{I}$ represents the mean intensity, N+1 is the number of data points t =0,$\cdots$,N and Δt is the time lag. All auto-correlation functions displayed in Fig. 12.7 (c,d) show a characteristic decay time of about 200 ms up to which a positive correlation persists. Once this characteristic time has elapsed, a channel that did emit above the average current is exhausted for some time which is reflected in a negative correlation, maintained for about one second. It is followed by a correlation function that is zero for all longer times, as expected. As a consistency check for the picture drawn above, we also investigated the cross-correlation between different ion emission spots. Neighbouring spots separated by only 10 nm experience the same local over- respectively under-supply. This signifies that they are supplied by joined pathways in the bulk. In fact, the build-up respectively decay of this supply is associated with a characteristic time during which a positive cross-correlation is maintained (Fig. 12.7 (e)). This decay time again amounts to 200 ms, consistent with the results of the auto-correlation experiments. However, spots that are separated by more than 100 nm show no correlation for any time (Fig. 12.7 (f)).

To obtain information about the lateral extent of the ion pathway network, we have finally investigated the distance dependence of the cross-correlation coefficient for Δt=0 as a function of the separation of two spots. The results are shown in Fig. 12.8. In accordance with the model, as sketched in Fig. 12.7 (a), the cross correlation gradually decays with increasing distance between two emission sites. A measure for the density of the network is given by the lateral distance over which a positive correlation between spatially separated ion channels is maintained. It turns out, as apparent from the distance decay of the cross correlation function for Δt=0 (Fig. 12.8 (d)), that individual ion pathways of the network *communicate* over distances up to about 60 nm.

[1] High brightness solid state ion generator, its use, and method for making such generator, Patent filed in March 2005. Invented by: C. Escher, S. Thomann, C. Andreoli and H.-W. Fink (University of Zurich), J. Toquant and D. Pohl (University of Basel)

[2] Vacuum Ion Emission from Solid Electrolytes: A novel source for Focused Ion Beams, C. Escher, S. Thomann, C. Andreoli and H.-W. Fink (University of Zurich), J. Toquant and D. Pohl (University of Basel), submitted to Appl.Phys.Lett.
[3] Direct Evidence for Conduction Pathways in a Solid Electrolyte, C. Escher, T. Latychevskaia and H.-W. Fink (University of Zurich), D. Pohl (University of Basel), submitted to Phys.Rev.Lett.
[4] .C. A. Angell, Annu. Rev. Phys. Chem. 43, 693 (1992).
[5] R. C. Agrawal, R. K. Gupta, J. Mat. Sci. 34, 1131 (1999).
[6] E.W. Mueller and T.T. Tsong, Field Ion Microscopy: Principles and Applications (New York: American Elsevier, 1969).
[7] C. Escher, S. Thomann, C. Andreoli, H.-W. Fink, J. Toquant and D.W. Pohl (submitted)
[8] J.P. Malugani, A. Wasniewski, M. Doreau, G. Robert and A. Al Rikabi, Mat. Res. Bull. 13, 427 (1978).
[9] M. Mangion and G.P. Johari, Phys.Rev. B39, 8845 (1987).
[10] J.D. Wicks, L. Börjesson, G. Bushnell-Wye, W.S. Howells and R.L. McGreevy, Phys. Rev. Lett. 74, 726 (1995).
[11] P. Mustarelli, C. Tomasi and A. Magistris, Phys. Rev. B 63, 144203 (2001).
[12] A. Bunde, K. Funke and M.D. Ingram, Solid State Ionics 86-88, 1311 (1996).
[13] J. Swenson, R.L. McGreevy, L. Börjesson and J.D. Wicks, Solid State Ionics 105, 55 (1998).
[14] J.E. Shelby and D.E. Day, J. Amer. Ceram. Soc. 52, 169 (1969).
[15] C.A. Angell, Chem. Rev. 90, 523 (1990).
[16] A.P. Sokolov, A. Kisliuk, M. Soltwisch and D. Quitmann, Phys. Rev. Lett. 69, 1540 (1992).
[17] C. Rousselot et al., Solid State Ionics 78, 211 (1995).
[18] J.H. Lee and S.R. Elliott, Phys. Rev. B 54, 12109 (1996).
[19] E. Kartini et al., Phys. Rev. B 61, 1036 (2000).

12.6 Teaching

Hiroshi Okamoto, Cornel Andreoli and Hans-Werner Fink

In connection with the new lecture *Physics on the nanometer scale* a new field emission microscope has been set-up in the framework of the advanced practical student courses in physics where the motion of Cs atoms on a W (110) surface can be observed and analyzed by field emission microscopy. The students observe field emission in an ultra high vacuum environment and learn how to measure the work function as well as to extract the tip radius of the field emitter from a Fowler-Nordheim plot. A change of the workfunction after Cs deposition onto the W-tip will be observed and the noise fluctuation of the field emission process is recorded with a spectrum analyzer to determine the diffusion constant of Cs on the W surface at different temperatures.

In addition 3 physical laboratory assistant apprentices spent part of their practical education course within our lab and were guided and advised by Cornel Andreoli.